Diamond & Related Materials 75 (2017) 91–95

Contents lists available at ScienceDirect

Diamond & Related Materials

journal homepage: www.elsevier.com/locate/diamond

Low turn-on field nanodiamond conic field emitter

Tingting Hao [a], Wuxia Li [a,*], Zhe Liu [a], Yu Sun [a], Ling Jin [a], Junjie Li [a], Changzhi Gu [a,b,c,**]

[a] Beijing National Lab of Condensed Matter Physics, Institute of Physics, Chinese Academy of Sciences, Beijing 100190, China
[b] Collaborative Innovation Center of Quantum Matter, Beijing 100190, China
[c] School of Physical Sciences, CAS Key Laboratory of Vacuum Physics, University of Chinese Academy of Sciences, Beijing 100190, China

ARTICLE INFO

Article history:
Received 11 November 2016
Received in revised form 19 January 2017
Accepted 9 February 2017
Available online 14 February 2017

Keywords:
Field emission
Low turn-on field
Nanodiamond cone
Field emitter

ABSTRACT

Field emission properties of individual nanocrystalline diamond cones with higher sp^2 content were investigated using a double-probe scanning electron microscope system. The nanodiamond cones were fabricated utilizing gray-scale patterns with a focused-ion-beam (FIB) system. The as-formed nanocones with slicing number of 150 have high content of sp^2 amorphous carbon surfaces and thus show a high emission current up to 54 μA at an applied voltage of 10 V. In addition, twice higher emission current was achieved by UV illumination under even lower turn-on field (1.1 V/μm), which benefits the realization of high performance cold cathode field emitters and UV detectors using such nanostructures.

1. Introduction

Nanodiamond as nanostructured materials has extinguished electronic, photonic and quantum properties and has shown unique advantages as candidate in cold cathode field emission applications [1]. Accordingly, intensive studies have been carried out based on nanodiamond films [2–4], shaped 1D nanodiamond structure [5,6]. According to these studies, nanodiamond has high emission behavior because the high sp^2 carbon component on the grain boundaries provides substantial transport channels for electrons [7]. Then, to get better field emission properties, we can realize it not only by the doping or surface morphology, but also with the introduction of the high content sp^2 carbon. This can be another way to improve the field emission and the application of carbon-based cold cathodes for vacuum electronics.

The hybrid system sp^2 carbon/diamond, which is the sp^2-coordinated with C-sp^3, has been researched by many groups, like the carbon nanotube decorated by nanodiamonds [8–11], hybrid diamond-like carbon and carbon nanotube [12,13], hybrid ultrananodiamond with carbon nanofiber [14] and even the hybrid graphene and diamond system [15]. It's great that all the results of the hybrid system showed the high emission ability and stable currents, but in the present development, the growth methods are mostly based on the Plasma Enhanced (PE) and hot filament (HF) chemical vapor deposition technique, which will bring the uncontrolled surface morphology, the burn-out under the high field due to high aspect ratio and formation of the hybrid material in a few subsequent steps. So here we propose a new method to get the hybrid system sp^2 carbon/diamond using FIB system.

All the time, FIB etching will bring the amorphization, Ga ions injection, which are seen as bad influence on the material, but it has recently been demonstrated that irradiation by energetic beam, especially when combined with heat treatment, can sometimes have beneficial effects on nanostructured materials, especially carbon material [16]. So here we apply the influence to get the hybrid system C/diamond using FIB, which will bring some advantages compared with other fabrication methods, like reactive ion etching and the CVD methods. The merits are shown, such as arbitrary shape acquisition with the high flexibility [17]; getting the different degree of sp^2 carbon varying with the fabrication time or dose simply [18]; easily modifying the surface state by Ga ion irradiation [19]; realizing the in-situ fabrication and measurement by integrating the measurement system with ease. The beneficial of FIB processing also includes the negligible force and heat imposed on a target, excellent beam positioning accuracy, large depth of focus and stable operating conditions [17]. But it has some disadvantages as well, like the formation of the sag structure, the low etching efficiency to the hard material, the unobtainable ultrafine tip, these may become the reasons of the poor emission behavior compared to other methods, and more efforts will be paid to get the high emission ability.

In this work, we realized the growth of the nanocrystalline diamond films and the fabrication of individual nanodiamond cones by FIB-milling related gray-scale nano-patterning. Field emission properties of individual nanocrystalline diamond cones were investigated using a double-probe scanning electron microscope system. The as-formed nanocones with slicing number of 150 had high content of sp^2

* Corresponding author.
** Correspondence to: C. Gu, Beijing National Lab of Condensed Matter Physics, Institute of Physics, Chinese Academy of Sciences, Beijing 100190, China.
E-mail addresses: haotingting@iphy.ac.cn (T. Hao), liwuxia@aphy.iphy.ac.cn (W. Li), czgu@aphy.iphy.ac.cn (C. Gu).

http://dx.doi.org/10.1016/j.diamond.2017.02.010
0925-9635/

amorphous carbon surfaces and thus showed a high emission current up to 54 μA at an applied voltage of 10 V. By UV illumination, twice higher emission current was achieved under even lower turn-on field (1.1 V/μm). These results suggest that the fabrication of nanoconic field emitters out of nanocrystalline diamond films by FIB-milling related gray-scale nano-patterning could be a potential approach for the realization of hybrid C/diamond system, high performance cold cathode field emitters and UV detectors.

2. Experimental procedure

For nanodiamond film deposition with the bias-assisted hot filament chemical vapor deposition (HFCVD) method, a silicon (100) wafer was used as the substrate. The deposition conditions were controlled strictly, in details, the gas flow volume ratio of the hydrogen and methane was 150 sccm: 10.5 sccm, the pressure was 2000 Pa, the Ta filament power was 7 kW, the distance between the sample and the filament was set at 14 mm. Using these deposition conditions, nanodiamond films with thickness of about ~20 μm, grain size around 50 nm were grown with a deposition rate of about 1.4 μm/h. A dual beam FIB-SEM (Helios 600i, FEI) system with liquid gallium ion source was used for nanocone fabrication. The used beam energy was 30 keV and the ion beam currents were in the range of 1.1 pA–69 nA. In-situ SEM imaging was conducted to monitor the shape and geometry evaluation of the resulted structures.

Direct-patterning of nanodiamond cones without any auxiliary gas but high resolution, time saving and excellent structure morphology was achieved using the Gray-scale pattern (GSP) approach, which includes a number of bitmap patterns with different gray scales information. For instance, in Fig. 1(a) equal-slicing method (ESM) was used to define the GSP, that is the slicing distance along the cone height direction even from the top to the bottom. Here the slicing number was N, it's not hard to imagine the pattern of each layer was a ring with an inner diameter and outer diameter. With lowering in the z-direction, increasing of the inner diameter while decreasing of the outer diameter of the ring was used in each layer. For the i^{th} slicing, the corresponding donut was A_iB_i and the inner and outer radii of it were R_{ii} and R_{io}, respectively. From the side view of the cone, a math description can be used to define the profile by coding in Matlab software with setting the inner and outer radius in each layer as desired, e.g. $R_{ii} = i/3 + 6$, $R_{io} = 256 - 4 * i/3$, then in the i^{th} layer, the gray scale value of 255 was assigned to the bitmap pattern (which presents the maximum dwell time in system) in area that $R_{ii} < R_i < R_{io}$, and in other area, the gray scale value was 0. Based on this, bitmap patterns defined by a certain layer number N can be formed and part of a typical bitmap pattern is shown in Fig. 1(b). As illustrated in Fig. 1(a), (b), by tuning N, the relationship of the R_{ii} and R_{io}, cones with different dimensions and slope angles can be achieved. After pattern design, the GSP was imported to the FIB system in order and appropriate fabrication conditions were optimized by considering the accelerating voltage, the current, and the dwell time of the ion beam to match the geometry, size and morphology of the desired nanocones.

In this work, for improved detection ability of the field emission properties, nanocones with wide oblique smooth surface are preferred. Nanodiamond cones with bottom diameter of 2.0 μm, cone angle of 38°, and height of 3.0 μm were fabricated with designated slicing number N of 150, an overall processing area of 10 μm × 10 μm with the thickness of each layer was set to be of 20 nm. Before processing, a layer of 40 nm Au was thermally evaporated onto nanodiamond film to increase the electrical conductivity for charging effect elimination. The used processing accelerating voltage of the beam was 30 kV and the ion beam current was 0.79 nA. After processing, the residual Au film was removed by wet chemical etching with Au corrosive liquid (KI: I: water = 115 g: 65 g: 100 ml). As a result, nanodiamond cone arrays with controllable inter-distance and uniform cone angle, height, and dimension can be obtained readily. Fig. 1(c) shows the typical SEM image of the fabricated cones.

Micro-Raman spectra were collected by scanning from 600 cm^{-1} to 2000 cm^{-1} with a commercial Raman scattering apparatus (mps 3000, Laser Quantum excitation laser wavelength 532 nm, excitation power ~ 1 mW). Field emission measurement was performed with a customized two-probe scanning electron microscope system connected to a Keithley 2450 electrical measurement system. The two probes were set 120° relative to each other and 30° to horizontal. The movement of the probes aligned with cardan joint can be controlled along x, y, z by manually rotating the fine screw with calculation accuracy of about 1 μm. With the sample stage that can be moved in five axis, x, y, z tilt and rotation, by tilting the stage 60° to horizontal, the probes were set perpendicular to the sample surface and the distance between the probe and the sample can be readily controlled by coarse tuning of sample stage and the fine tuning of the probe. The base pressure during measurement was below 5×10^{-4} Pa. The electron beam accelerating voltage used was 30 kV and the filament current was 100 μA. The probes were very fine W tips, which were obtained by the electrochemical etching with KOH aqueous solution, the apex radius of the tip was as fine as a hundred of nanometers. And the UV illumination was realized by introducing a UV light source (NBET, Radiant output power 50 W, spectral output power 200 nm–2500 nm) into such vacuum system with the optical filter getting the certain width of the wavelength.

3. Results and discussion

To understand the effect of ion beam irradiation, Raman scattering spectra were collected on the as-grown film, FIB-proceeded cones with different slicing numbers. Raman scattering is sensitive to carbon-carbon bonding states, thus it was used to characterize the carbonaceous materials. Fig. 2 shows the corresponding micro-Raman spectra. The main spectral lines that centered at 1138 cm^{-1} and 1479 cm^{-1} are often originated from nanodiamond, which have been attributed to the trans-(CH)x (trans-polyacetylene) at the grain boundaries [20], while peaks centered at 1357 cm^{-1} (D band) and 1548 cm^{-1} (G band) manifest carbon atom lattice defects and sp^2 hybrid carbon atom stretching vibration in the plane, which indicate the coating of sp^2 carbon with disordered and ordered graphitic structures on the

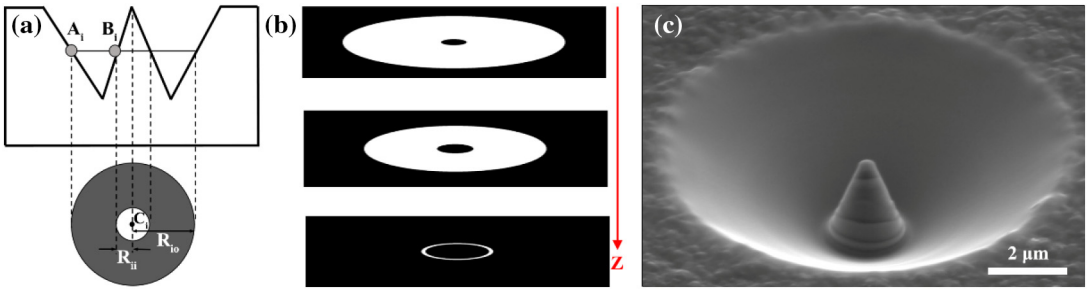

Fig. 1. Fabrication of nanocrystal diamond cones: (a) the scheme of the cone cross-section used for gray-scale patterning based on FIB milling; (b) the illustration of the selected bitmap pattern series for FIB gray-scale patterning; (c) a typical SEM image of the fabricated cones.

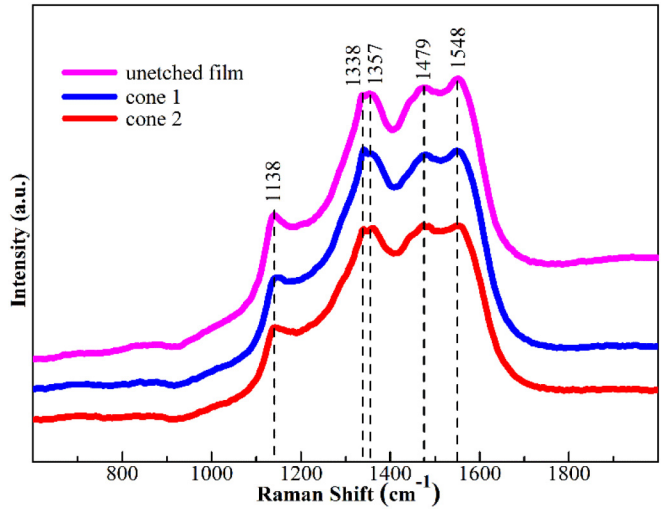

Fig. 2. Micro-Raman spectra of unprocessed nanocrystal diamond film (pink), cone fabricated with slicing number N of 120 (cone1, blue) and slicing number N of 150 (cone 2, red). (For interpretation of the references to colour in this figure legend, the reader is referred to the web version of this article.)

diamond cone surface [21]. A sharper diamond peak centered at ~1338 cm^{-1} can be distinguished from the broader graphitic D peaks, which reveals that the as-formed cone is composed of a nanodiamond core and a cover of amorphous carbon with high-content of sp^2 bonding, which was simultaneously formed during cone fabrication process. But from the peak intensity we can get that the graphite-like carbon is the major ingredient. The sp^2 content mainly comes from the high density of grain boundaries, FIB fabrication and impurity at the interface between the nanodiamond film and the silicon substrate during the early stage of film growth. From the comparison of these major spectral lines, $I_{diamond}/I_G$ ratio reflects the structural change to some degree, though the Raman spectral is not exact in the quantitative analysis. From Fig. 2, it can be seen that the corresponding $I_{diamond}/I_G$ ratio of the un-etched film, the diamond cone etched by FIB, with slicing number *N* of 120 and 150, are 0.230, 0.191 and 0.132, respectively. The ratio decreases slightly, which indicates that mild introduction of defects and increasing of the sp^2 content cannot be avoided during cone fabrication. It's worth noting that the time of the ion beam irradiation will slightly infect the content of the graphitization.

The field emission measurement was conducted on individual nanocones (slicing number *N* is 150). The tip-probe measurement setup is shown in Fig. 3(a), in our setup, the actual distance between the nanocone tip and the probe can be finely manually controlled as narrow as to hundred nanometers, which guaranteed the higher collection efficiency of the emission current as obtained in our experiment. The emission current curve is shown in Fig. 3(b). A quick rise can be seen at an applied voltage of about 4.8 V and the emission current was about 54 μA when an voltage of 10 V was applied. For better understanding, $\beta E = V/R_{tip}$ was used for quantitatively interpretation [22]. Here β is the field enhancement factor, *E* is the electrical field, V is the applied voltage and R_{tip} is the tip radius of curvature. The turn-on electrical field of one measured cone is derived to be of 1.3 V/μm, a point that is corresponding to a current density of 10 μA/cm^2. β can be described as $2.1(h/r + 0.8)^{0.73}$ from the β model [23], thus in our case, it is about 22 for a cone with height of 3.0 μm and cone apex radius r of 125 nm. Here, the area used for current density calculation was the whole area of the fabricated nanocone. Actually, the area of the emission was smaller than that used in our calculation, which suggested a possible even higher emission current density. Although the emission current value is lower than the value of the carbon nanotube/nanodiamond hybrid system, with emission current density 6 mA/cm^2 at applied field E of 6.2 V/μm [9], the reason of it is the lower applied voltage and β, but the turn-on field is a bit lower than that got from the other system, for example, arrays of conical-shaped nanodiamond structures formed by single-step CVD process was about 15 V/μm [24] and the free-standing graphene-diamond hybrid film was 2.4 V/μm [15]. The lower turn-on filed and higher emission current we obtained are mainly due to the reasons that: firstly, the conical structure can effectively increase the emission field than other surface structure; secondly, the amorphous carbon,which came from the ion beam irradiation and film deposition process, can substantially increase the electron hopping conduction through the defect bands with the wide band-gap of local sp^3 sites in the cascaded sp^2-sp^3-sp^2 surface nanostructure; thirdly, nanodiamond has increased grain boundaries, which can also enhance the field emission [25]; and finally, this measurement setup with the ultra-short two probes distance can greatly improve the efficiency of collection.

The nanodiamond cone emission was further explored using a simplified Fowler-Nordheim (FN) theory, which is described with the following equation:

$$I/V^2 = A \exp\left(-B\varphi^{3/2}/\beta V\right) \quad (1)$$

Here φ is the surface work function, $B = 6.831 \times 10^3\ eV^{-3/2}\ V\ \mu m^{-1}$, β is the electrical field enhancement factor. Accordingly, the responding FN plot of the nanocones is shown in Fig. 3(b) in-set. It's worth noting

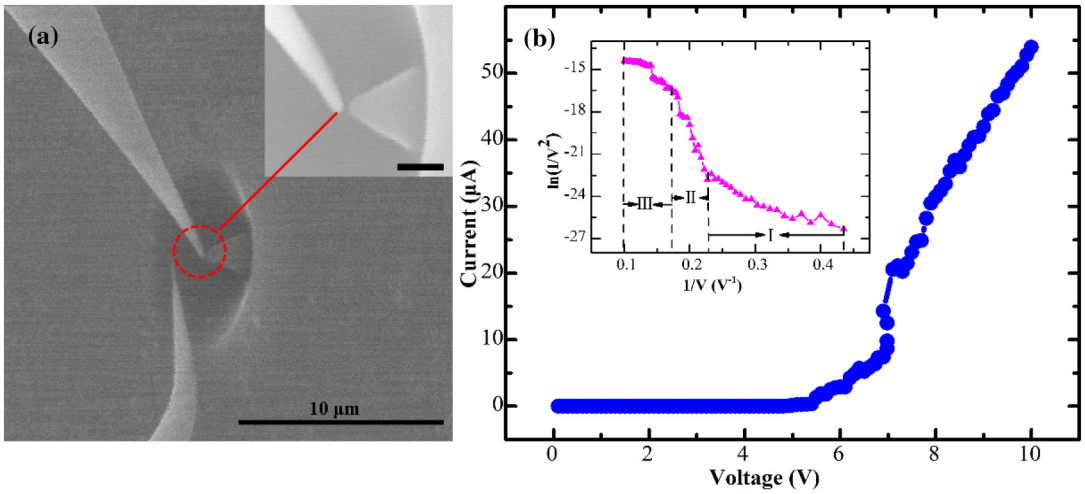

Fig. 3. The field emission properties of nanocones fabricated out of nanocrystalline diamond films: (a) the SEM image of the tip-probe measurement setup, the scale bar in the inset is 500 nm, the gap under SEM measurement is around 120 nm; (b) the I–V curve of the nanodiamond cone and the inset is the corresponding F–N plot.

that the F—N plot has different slopes, which represents the different emission behavior. In the unstable emission region I (in voltage range of 0–3.8 V), the emission is not well conformed to typical FN theory, which comes from the sp^2 content [15]. In the emission region II (in voltage range of 3.8–5.8 V), FN plot shows good linearity with a constant, which indicates the emission well conforming to FN-type electrons vacuum tunneling and comes from the grain boundaries of nanodiamond and the high sp^2 content. From the left of the F—N plot III (in voltage range of 5.8–10 V), the slope has a decrease, this may be a sign of the degradation of emission for this cone [21], a surface desorption process induces the decrease of the effective work function, or the burning (or evaporation) of effective local emission spots in the grain boundary occurs, which will reduce the field enhancement factor β [26].

Based on Eq. (1), the slope S for FN plot at the stable emission is given as:

$$S = \left| \frac{d\left(\ln\left(I/V^2\right)\right)}{d(1/V)} \right| = \frac{B}{\beta}\varphi^{3/2} \tag{2}$$

Based on the stable emission area II of the FN plot, for our individual nanocones, the β is almost constant, then the work function maintains at a stable value since $S \propto \varphi^{3/2}$. By calculating, the surface effective work function of the nanocone was estimated to be of 0.4 eV, which is a little low value. There are two reasons shown as below: firstly, the field emission of hybrid C/diamond system is controlled by many effects, one of them is the ballistic phonon drag of electrons, which brings an internal thermoelectric field due to the temperature difference inside the emission area [8,27,28], the emission center is at least 20 times smaller than the total emitter area, like the grain size d ≈ 100 nm, the local field $E_{loc} \approx 10^6$ V/cm and if the emission center is taken to be 10 times smaller, the local field will increase by a factor of 1000 [27]. In our experiment, the grain size is not more than 50 nm, the local field is enough large to induce an appreciable thermoelectric field, which will highly decrease the effective work function. Secondly, Ga ion irradiation can form the defect in the material, the defect band formation moves the Fermi level towards the conduction band, and thus decreases the work function [6].

The field emission of cones fabricated with slicing number *N* of 120, has also been measured, which can be seen in Fig. 4. The results show that the turn-on field (2.0 V/μm) and emission current 12.0 μA with an applied voltage of 10.0 V have decreased as well, which further shows the FIB processing has non-negligible influence on the surface state. And it maybe predict if the slicing number increases to a value, it will bring the poor field emission property, because the nanodiamond-cone may become non-crystallization completely.

Furthermore, the effect of UV light on the field emission properties of nanocones (the slicing number *N* is 120, 150) were examined by shedding an UV light with wavelength from 200 nm to 500 nm to the cone under measuring. Fig. 4 shows the current as a function of the applied field in the dark and under the illumination. The turn-on electrical field of the cone with the slicing number of 120 in the dark field and under the illumination at current density of 10 μA/cm^2 is 2.0 V/μm and 1.3 V/μm, respectively. The turn-on field under UV decreased dramatically. And by comparison, as slicing number increases to 150, the turn-on electrical field under UV also decreases to 1.1 V/μm, due to the increased surface carbon. The current densities of both them are also higher with illumination, since electron-hole pairs are generated due to the photoelectric effect and the excited electrons move into the valence band, which can fascinate the electron emission when the electrical field is applied into the conical structures. In other word, the UV illumination can result in energy band bending to a lower level for electrons to tunnel easier to form emission current. The electrons thus accumulate in the conical tip and then can cause discharge and reduce the turn-on field [29].

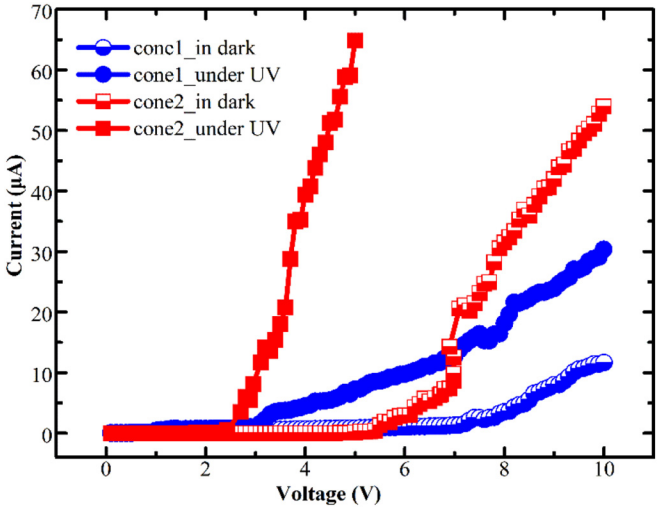

Fig. 4. The field emission properties of nanodiamond cone structures (3.0 μm in height, 2.0 μm in diameter at the base), which are fabricated with slicing number N of 120 (cone1, blue) and 150 (cone2, red) in dark (semi-solid) and under UV illumination (solid), respectively. (For interpretation of the references to colour in this figure legend, the reader is referred to the web version of this article.)

4. Conclusion

In summary, nanocrystalline diamond films have been grown on Si substrates and fine cones with high sp^2 content have been fabricated out of such material with gray-scale pattern based on FIB-milling. Micro Raman Spectroscopy shows that the as-formed nanocones have high content of sp^2 amorphous carbon surfaces. Field emission properties of individual nanocones with different slicing numbers were investigated using a double-probe scanning electron microscope system with and without UV illumination, the results show the increasing slicing number and the introduction of UV can improve the emission. Although the emission current is a little bit low, the easy fabrication method and excellent fabrication character suggest high content sp^2 carbon nanocone fabrication using GSP related FIB-milling based on nanocrystalline diamond could be a potential approach for high performance carbon-based cold cathode field emitters and UV detectors.

Acknowledgments

This work is supported by the National Natural Science Foundation of China under Grants Nos. 51272278, 61390503, 91323304, 11574369 and 11574368; XDB07020200, and The National Key Research and Development Program of China under Grant No. 2016YFA0200400.

References

[1] M.L. Terranova, S. Orlanducci, M. Rossi, E. Tamburri, Nanodiamonds for field emission: state of the art, Nanoscale 7 (2015) 5094–5114.
[2] S. Raina, W.P. Kang, J.L. Davidson, Field emission from nanodiamond grown with 'ridge' type geometrically enhanced features, Diamond Relat. Mater. 17 (2008) 790–793.
[3] S.G. Wang, Q. Zhang, S.F. Yoon, J. Ahn, Q. Zhou, Q. Wang, D.J. Yang, J.Q. Li, S. Zhang Shanyong, Electron field emission enhancement effects of nano-diamond films, Surf. Coat. Technol. 167 (2003) 143–147.
[4] X.C. LeQuan, W.P. Kang, J.L. Davidson, M. Guo, B.K. Choi, Micro-Raman, SEM, XPS, and electron field emission characterizations of nitrogen-induced shallow defects on nanodiamond films fabricated with different growth parameters, Diamond Relat. Mater. 18 (2009) 191–195.
[5] K. Subramanian, W.P. Kang, J.L. Davidson, J.D. Jarvis, W.H. Hofmeister, B.K. Choi, M. Howell, Geometrical field enhancement on micropatterned nanodiamond film for electron emissions, Diamond Relat. Mater. 15 (2006) 417–425.
[6] A. Wisitsora-At, W. Kang, J. Davidson, D. Kerns, A study of diamond field emission using micro-patterned monolithic diamond tips with different sp^2 contents, Appl. Phys. Lett. 71 (1997) 3394–3396.

[7] K.Y. Teng, H.C. Chen, H.Y. Chiang, C.C. Horng, H.F. Cheng, K.J. Sankaran, N.H. Tai, C.Y. Lee, I.N. Lin, The role of nano-graphite phase on the enhancement of electron field emission properties of ultrananocrystalline diamond films, Diamond Relat. Mater. 24 (2012) 126–133.
[8] A. Vul, K. Reich, E. Eidelman, M.L. Terranova, A. Ciorba, S. Orlanducci, V. Sessa, M. Rossi, A model of field emission from carbon nanotubes decorated by nanodiamonds, Adv. Sci. Lett. 3 (2010) 110–116.
[9] V. Guglielmotti, S. Chieppa, S. Orlanducci, E. Tamburri, F. Toschi, M.L. Terranova, M. Rossi, Carbon nanotube/nanodiamond structures: an innovative concept for stable and ready-to-start electron emitters, Appl. Phys. Lett. 95 (2009) 222113.
[10] D. Varshney, B.R. Weiner, G. Morell, Growth and field emission study of a monolithic carbon nanotube/diamond composite, Carbon 48 (2010) 3353–3358.
[11] S. Orlanducci, E. Tamburri, M.L. Terranova, M. Rossi, Nanodiamond-coated carbon nanotubes: early stage of the CVD growth process, Chem. Vap. Depos. 14 (2008) 241–246.
[12] H. Zanin, P.W. May, M.H. Hamanaka, E.J. Corat, Field emission from hybrid diamond-like carbon and carbon nanotube composite structures, ACS Appl. Mater. Interfaces 5 (2013) 12238–12243.
[13] H. Kinoshita, I. Ippei, H. Sakai, N. Ohmae, Synthesis and mechanical properties of carbon nanotube/diamond-like carbon composite films, Diamond Relat. Mater. 16 (2007) 1940–1944.
[14] X. Xiao, O. Auciello, H. Cui, D.H. Lowndes, V.L. Merkulov, J. Carlisle, Synthesis and field emission properties of hybrid structures of ultrananocrystalline diamond and vertically aligned carbon nanofibers, Diamond Relat. Mater. 15 (2006) 244–247.
[15] D. Varshney, C.V. Rao, M.J.F. Guinel, Y. Ishikawa, B.R. Weiner, G. Morell, Free standing graphene-diamond hybrid films and their electron emission properties, J. Appl. Phys. 110 (2011) 044324.
[16] A.V. Krasheninnikov, F. Banhart, Engineering of nanostructured carbon materials with electron or ion beams, Nat. Mater. 6 (2007) 723–733.
[17] Q. Jiang, D. Liu, G. Liu, Y. Chang, W. Li, X. Pan, C. Gu, Focused-ion-beam overlay-patterning of three-dimensional diamond structures for advanced single- photon properties, J. Appl. Phys. 116 (2014) 044308.
[18] R. Brunetto, G.A. Baratta, G. Strazzulla, Amorphization of diamond by ion irradiation: a Raman study, J. Phys.: Conf. Ser. 6 (2005) 120–125.
[19] W.J. MoberlyChan, D.P. Adams, M.J. Aziz, G. Hobler, T. Schenkel, Fundamentals of focused ion beam Nanostructural processing: below, at, and above the surface, MRS Bull. 32 (2011) 424–432.
[20] P. Sun, C. Tang, X. Xia, Z. Yao, B. Quan, G. Yuan, C. Gu, J. Li, Controlled fabrication of periodically high-aspect ratio CVD-diamond nanopillar arrays by pure oxygen etching process, Microelectron. Eng. 155 (2016) 61–66.
[21] Q. Wang, Z.L. Wang, J.J. Li, Y. Huang, Y.L. Li, C.Z. Gu, Z. Cui, Field electron emission from individual diamond cone formed by plasma etching, Appl. Phys. Lett. 89 (2006) 063105.
[22] C.T. Hsieh, J.M. Chen, H.H. Lin, H.C. Shih, Field emission from various CuO nanostructures, Appl. Phys. Lett. 83 (2003) 3383–3385.
[23] C. Edgcombe, U. Valdre, Experimental and computational study of field emission characteristics from amorphous carbon single nanotips grown by carbon contamination. I. Experiments and computation, Philos. Mag. B 82 (2002) 987–1007.
[24] S. Orlanducci, V. Guglielmotti, I. Cianchetta, V. Sessa, E. Tamburri, F. Toschi, M.L. Terranova, M. Rossi, One-step growth and shaping by a dual-plasma reactor of diamond nanocones arrays for the assembling of stable cold cathodes, Nano.Sci. Nanotech. Let. 4 (2013) 338–343.
[25] K.J. Sankaran, S. Kunuku, K.C. Leou, N.H. Tai, I.N. Lin, Enhancement of the electron field emission properties of ultrananocrystalline diamond films via hydrogen post-treatment, ACS Appl. Mater. Interfaces 6 (2014) 14543–14551.
[26] Y.L. Li, J.J. Li, Q. Wang, C.Z. Gu, Local field electron emission from grain bound- aries of CVD diamond film, Diamond Relat. Mater. 18 (2009) 229–231.
[27] A.T. Dideykin, E.D. Eidelman, A.Y. Vul, The mechanism of autoelectron emission in carbon nanostructures, Solid State Commun. 126 (2003) 495–498.
[28] N. Neugebohrn, T. Sun, F.A.M. Koeck, G.G. Hembree, R.J. Nemanich, T. Schmidt, J. Falta, Spatial correlation of photo-induced and thermionic electron emission from low work function diamond films, Diamond Relat. Mater. 40 (2013) 12–16.
[29] S.J. Young, Y.H. Liu, Enhanced field emission properties of two-dimensional ZnO nanosheets under UV illumination, IEEE J. Sel. Top. Quant. 21 (2015) 427–430.